Research on
Engineering
Structures & Materials
journal homepage: http://jresm.org

RESEARCH
GROUP

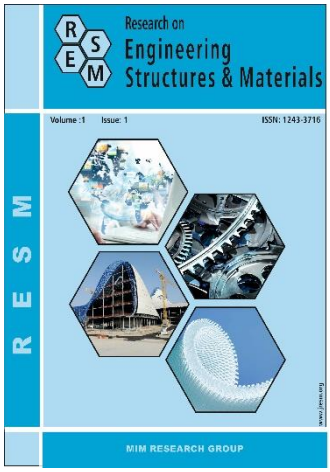

Darrieus vertical axis wind turbines: methodology to study the self-start capabilities considering symmetric and asymmetric airfoils

Nelson C. Batista, Rui Melicio, Victor M.F. Mendes

Online Publication Date: 28 Mar 2018
URL: http://dx.doi.org/10.17515/resm2017.39ds0108
DOI: http://dx.doi.org/10.17515/resm2017.39ds0108
Journal Abbreviation: *Res. Eng. Struct. Mat.*

To cite this article
Batista NC, Melicio R, Mendes VMF. Darrieus vertical axis wind turbines: methodology to study the self-start capabilities considering symmetric and asymmetric airfoils. *Res. Eng. Struct. Mat.*, 2018; 4(3): 189-217.

Research on Engineering Structures & Materials
journal homepage: http://jresm.org
MIM RESEARCH GROUP

Research Article

Darrieus vertical axis wind turbines: methodology to study the self-start capabilities considering symmetric and asymmetric airfoils

Nelson C. Batista[1,2], Rui Melicio[*,1,2,3], Victor M.F. Mendes[1,4,5]

[1] *Departmento de Física, Escola de Ciências e Tecnologia, Universidade de Évora, Portugal*
[2] *IDMEC, Instituto Superior Técnico, Universidade de Lisboa, Lisbon, Portugal*
[3] *ICT, Universidade de Évora, Portugal*
[4] *Department of Electrical Engineering and Automation, Instituto Superior de Engenharia de Lisboa, Portugal*
[5] *CISE, Electromechatronic Systems Research Centre, Universidade da Beira Interior, Portugal*

Article Info

Article history:
Received 01 Jan 2018
Revised 25 Feb 2018
Accepted 26 Mar 2018
Keywords:

Self-starting,
Blade profile,
Symmetric airfoil,
Asymmetric airfoil,
Vertical axis wind turbines

Abstract

The rapid growth of wind power generation and the need for a smarter grid with decentralized energy generation has increased the interest in vertical axis wind turbines (VAWT), especially for the urban areas. For the urban areas the VAWT offer several advantages over the horizontal ones, so their acceptance is rising. The lift-type VAWT (Darrieus wind turbines) have a natural inability to self-start without the help of extra components. The existing methodologies are usually used to optimize the wind turbine performance, but not its ability to self-start. Indeed, studying the aerodynamic behavior of blade profiles is a very complex and time-consuming task, since blades move around the rotor axis in a three-dimensional aerodynamic environment. Hence, a new methodology is presented in this paper to study the self-start ability of VAWT, which offers a substantial time reduction in the first steps of new blade profiles development. Both symmetrical and asymmetrical airfoils are targeted in our study, presenting comprehensive results to validate our methodology.

Introduction

The renewable energies share in power production has increased significantly in many European countries [1-6]. The wind energy systems have been considered as one of the most cost effective of all the currently exploited renewable energy sources, so a growing investment in wind energy systems has occurred in the last decade.

The decentralized energy generation is an important solution in a smarter grid with a growing acceptance for the urban areas. Also, the increasing need for more environmentally sustainable housing and the new European norms regulating this issue, have contributed for the promotion of wind energy systems in buildings.

In urban areas the wind is very turbulent and unstable with fast changes in direction and velocity.

*Corresponding author: ruimelicio@gmail.com
DOI: http://dx.doi.org/10.17515/resm2017.39ds0108

In these environments the vertical axis wind turbines (VAWT) have several advantages over horizontal axis wind turbines (HAWT) [7]: insensitivity to yaw wind direction changes (so the turbine does not need the extra components to turn the rotor against the wind); smaller number of components (the reduced number of components leads to a more reliable product and a reduced cost in production and maintenance); very low sound emissions (ideal for urban areas); ability to generate energy from wind in skewed flows (skewed flows are very usual in urban areas, especially in the rooftop of buildings); three dimensional structural design, easier to integrate in urban architecture; ability to operate closer to the ground level.

The modern VAWT can be divided in three basic types: Savonius [8-9], Darrieus [10-11] and H-rotor [12]. The Savonius VAWT is a drag-type wind turbine. This type of wind turbine has the ability to self-start and has high torque, but it operates at low tip speed ratio (TSR). The Darrieus VAWT is a lift-type wind turbine. Darrieus VAWT can be divided in two kinds: curved bladed turbine (or egg-shaped turbine) and straight bladed turbine. The H-rotor is the most common configuration of the straight bladed Darrieus VAWT. The "H" rotor received its name due to the arms and straight blade configuration resembling the "H" letter. Lift-type wind turbines can operate at high TSR, but they usually have an inherent problem: the inability to self-start [13]. On one hand, if VAWT need to be self-starting capable their performance is compromised, not being able to work at high TSR. On the other hand, if VAWT need to exhibit superior performance at high TSR they are not able to self-start without extra components or external power.

This paper is based on straight bladed Darrieus VAWT and the main goal is to present a new methodology to study their self-start behavior, capable of offering a fast tool for developing blade profiles. In this methodology, a relationship between the wind turbine (when it's in a stopped position), its blade profile design, and the aerodynamic behavior of the wind flow, is determined. Several symmetrical and asymmetrical airfoils are tested and their output data analyzed in order to demonstrate the proficiency of the new methodology.

This paper is organized as follows. Section 2 presents the performance prediction and modeling of the straight bladed Darrieus VAWT. Section 3 addresses the Darrieus VAWT ability to self-start. Section 4 provides the new methodology to study self-start capabilities. Section 5 presents the results considering several symmetrical and asymmetrical NACA airfoils. Finally, Section 6 outlines the conclusions.

2. Darrieus VAWT Performance Prediction and Modeling

The VAWT aerodynamic modeling is very complex since the turbine blades travel around the rotor in a 360º rotation. While some of the blades have lift forces acting on them, others suffer from drag forces in an opposing movement to the rotor rotation. Additionally, the blades that are traveling in the upstream side of the turbine induce some turbulence that will affect the blades performance travelling in the downstream side. These and other issues make VAWT performance prediction a very hard task, far more complex than for HAWT.

Several VAWT performance prediction models [13] have been developed, which will be briefly described in this section. The flow velocities diagram of a lift-type VAWT is shown in Fig. 1.

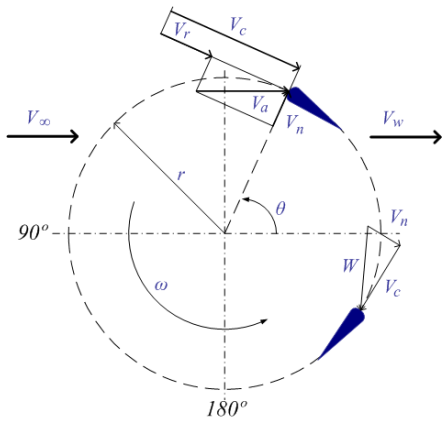

Fig. 1 Flow velocities diagram of a lift-type VAWT

In Fig. 1 shows the undisturbed wind velocity V_∞ that reaches the wind turbine, the induced velocity V_a at the blade profile level, and the induced velocity due to the rotor angular speed at the wind turbine V_r, i.e., due to the blade in its movement around the rotor, given by:

$$V_r = \omega r \tag{1}$$

The blade is influenced by the contribution of V_a and V_r to a resulting chordal velocity V_c, i.e., the velocity parallel to the chord line of the blade profile, given by:

$$V_c = V_r + V_a \cos\theta = r\omega + V_a \cos\theta = \lambda V_a + V_a \cos\theta \tag{2}$$

The induced velocity V_a has also a contribution to the normal velocity V_n, i.e., the velocity in a radial direction in relation to the center of the rotor, given by:

$$V_n = V_a \sin\theta \tag{3}$$

The relative flow velocity W is given by:

$$W = \sqrt{V_c^2 + V_n^2} = V_a \sqrt{1 + 2\lambda \cos\theta + \lambda^2} \tag{4}$$

The blade an angle of attack α is given by:

$$\alpha = \tan^{-1}\left(\frac{V_n}{V_c}\right) = \tan^{-1}\left(\frac{V_a \sin\theta}{r\omega + V_a \cos\theta}\right) = \tan^{-1}\left(\frac{\sin\theta}{r\omega/V_a + \cos\theta}\right) \tag{5}$$

If the blade turbine is able to modify its pitch angle γ, the blade angle of attack α will be given by:

$$\alpha = \tan^{-1}\left(\frac{\sin\theta}{r\omega/V_a + \cos\theta}\right) - \gamma \tag{6}$$

The forces diagram acting on the blade airfoil is shown in Fig. 2.

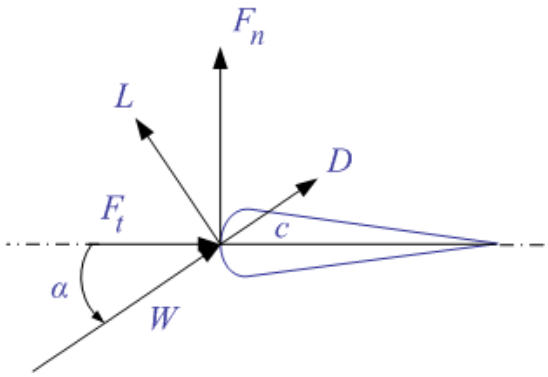

Fig. 2 Forces diagram acting on the blade airfoil

The tangential force coefficient C_t and the normal coefficient C_n are given by:

$$C_t = C_l \sin\alpha - C_d \cos\alpha \tag{7}$$

$$C_n = C_l \cos\alpha + C_d \sin\alpha \tag{8}$$

The tangential force F_t and normal force F_n are given by:

$$F_t = \frac{1}{2} C_t \rho\, c\, h\, W^2 \tag{9}$$

$$F_n = \frac{1}{2} C_n \rho\, c\, h\, W^2 \tag{10}$$

The average tangential force F_{ta} in function of the tangential force F_t around the rotor and the azimuth angle θ is given by:

$$F_{ta} = \frac{1}{2\pi} \int_0^{2\pi} F_t(\theta) d\theta \tag{11}$$

The turbine overall torque Q is given by:

$$Q = n\, F_{ta}\, r \tag{12}$$

The turbine overall power P is given by:

$$P = Q\,\omega \tag{13}$$

The power coefficient C_P is the relation between the wind turbine power output and the power available in the wind, given by:

$$C_P = \frac{P}{1/2\,\rho\,V_\infty{}^3 A} = \frac{n\,F_{ta}\,r\,\omega}{1/2\,\rho\,V_\infty{}^3\,h\,r^2} = 2\frac{n\,F_{ta}\,\omega}{\rho\,V_\infty{}^3 h\,r} \tag{14}$$

Several mathematical models have been developed by different researchers to achieve a more accurate prediction of lift-type VAWT performance. The most common used models can be divided in three categories: blade element momentum (BEM) model, vortex model and cascade model [13].

2.1. BEM Model

BEM theory is a combination of blade element theory with basic momentum theory, studying the flow and behavior of the air on the blades and the involved forces. The base models on the BEM theory experience some problems when trying to predict the performance for high TSR and high solidity σ turbines. Based on BEM theory, several models have been developed: single streamtube model, multiple streamtube model and double-multiple streamtube model.

2.1.1 Single Streamtube Model

This is the simplest model and is represented by a single streamtube where the turbine is placed and its blades in their revolution are translated in an actuator disc. All the blades are translated in only one blade where its chord is the sum of all turbine blades chords. The wind speed in the upstream and downstream sides of the rotor is assumed to be constant. The effects of the wind speed outside the streamtube are assumed negligible. The single streamtube model is illustrated in Fig. 3.

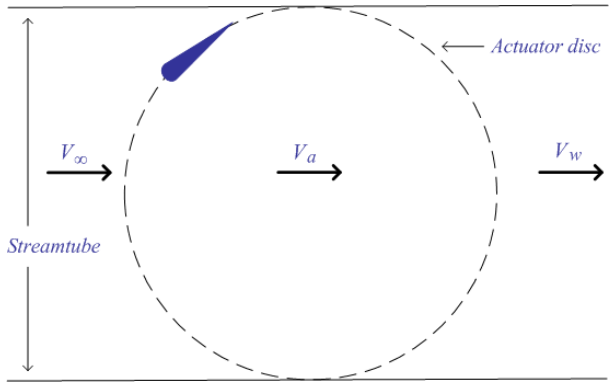

Fig. 3 Single streamtube model diagram

The uniform velocity through the rotor is given by:

$$V_a = \frac{V_\infty + V_w}{2} \tag{15}$$

The turbine drag force F_D considering the rate of change of momentum, is given by:

$$F_D = A\rho V_a (V_\infty - V_w) \tag{16}$$

The turbine drag coefficient C_D is given by:

$$C_D = \frac{F_D}{1/2\,\rho A V_a^2} = \frac{A\rho V_a (V_\infty - V_w)}{1/2\,\rho A V_a^2} = \frac{V_\infty - V_w}{1/2 V_a} \tag{17}$$

Considering (15), C_D is given by:

$$C_D = \frac{V_\infty - (2V_a - V_\infty)}{1/2 V_a} = \frac{4(V_\infty - V_a)}{V_a} \tag{18}$$

The induced velocity ratio is given by:

$$\frac{V_a}{V_\infty} = \frac{1}{1 + C_D/4} \tag{19}$$

By using (19), and with the general mathematical expressions that were presented before, it is now possible to predict the torque and power coefficient of the VAWT. However, the single streamtube model is not good in predicting the turbine performance, since it neglects the wind speed variations inside and outside the rotor, usually providing much higher values than those obtained from experimental data.

2.1.2 Multiple Streamtube Model

This model is a variation of the single streamtube model, where instead of having only one streamtube there are several parallel and adjacent streamtubes independent from each other, having their own undisturbed, induced and wake velocities. The multiple streamtube model is shown in Fig. 4.

The induced velocity ration equation for this model is given by:

$$\frac{V_a}{V_\infty} = 1 - \left(\frac{k}{2} \frac{nc}{r} \frac{r\omega}{V\infty} \sin\theta \right) \tag{20}$$

Several multiple streamtube models have been presented over the years, with the addition of drag forces, blade profile geometry, turbine solidity, curvature flow, and so on. However, the performance prediction is still far from experimental values.

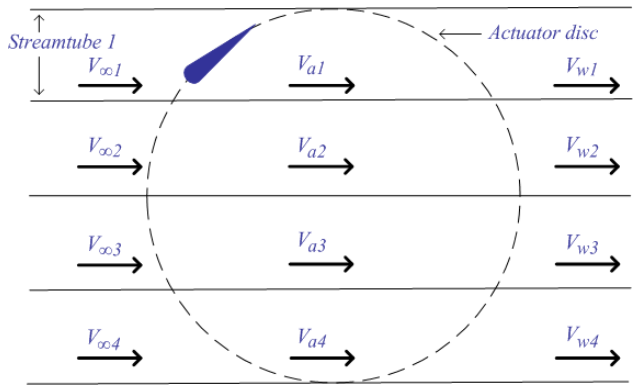

Fig. 4 Multiple streamtube model diagram

2.1.3 Double-Multiple Streamtube Model

The double-multiple streamtube model [14-16] is a variation of the multiple streamtube model, in which the actuator disc is divided into half cycles representing the upstream and the downstream of the rotor, as shown in Fig. 5.

The actuator disc is then divided in two actuator discs, each of them with their own induced velocity. The induced velocity in the upstream is represented by V_{au} and the induced velocity in the downstream is represented by V_{ad}.

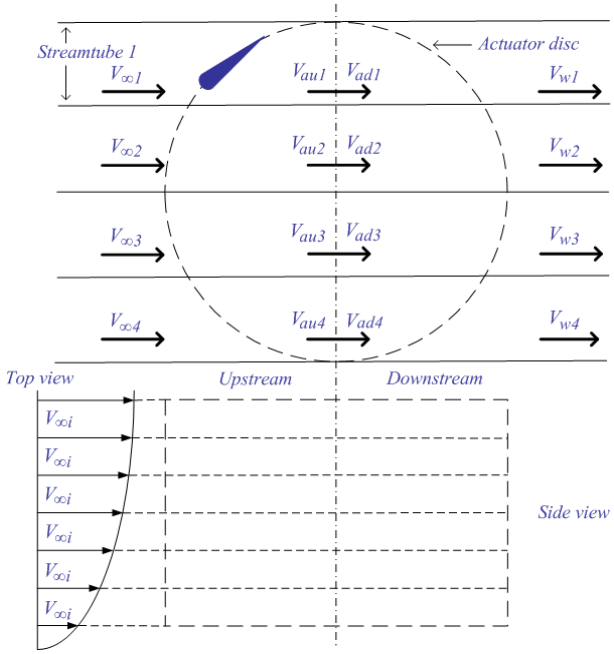

Fig. 5 Double-multiple streamtube model diagram

The induced velocity in the downstream is influenced by the wake velocity in the upstream V_e, which is given by:

$$V_e = V_{\infty i}\left(2\frac{V_{au}}{V_{\infty i}} - 1\right) = V_{\infty i}\left(2u_u - 1\right) \tag{21}$$

The induced velocity in the downstream V_{ad} is given by:

$$V_{ad} = u_d V_e = u_d\,(2u_u - 1)V_{\infty i} \tag{22}$$

The interference factor for the downstream, which is given by:

$$u_d = \frac{V_{ad}}{V_e} \tag{23}$$

This model has received some improvements over the years and provides a good performance for most predictions, but it may suffer convergence problems in some cases.

2.2. Vortex Model

The vortex model [17-18] predicts the performance of VAWT by calculating the vorticity in the wake of the blades. The blades are substituted by vortex filaments whose strengths will be determined by the blade profile coefficients, relative flow velocity and angle of attack. By Helmholtz theorems of vorticity, the strengths of the vortex filaments are equal to each trailing tip vortex.

Several modifications on this model have been presented, but the main disadvantage of the vortex model still persists, the high computation time.

2.3. Cascade Model

In the cascade model [19] the VAWT blades are arranged in vanes called cascade and positioned in equal interspaces of the turbine perimeter divided by the number of blades. The aerodynamic properties of the blades are calculated independently taking in consideration the upwind and downwind sides of the rotor, their local Reynolds number and the local angle of attack.

This model does not have convergence problems and provides good performance prediction in low and high TSR. However, like the vortex model, the cascade model requires a high computation time.

2.4. Aerodynamic Disturbances

Although there are several mathematical models for the VAWT performance prediction, still the aerodynamic behavior of the VAWT rotor is very difficult to predict. Several aerodynamic disturbances can be found in the VAWT operation, such as deep stall, dynamic stall and laminar separation bubbles.

References [20-22] model the dynamic stall on VAWT, validating the results with particle image velocimetry data. In the rooftops the wind flows in a skewed movement. Reference [23] addresses the feasibility analysis of a Darrieus VAWT installation in the rooftop of a building. Also, a computational study of a rooftop size VSWT with straight blades is presented in [24]. Some solutions have been presented for preventing vortex shedding and reducing drag in flows past bluff bodies. Large vortices forming in high-speed flows past bluff bodies tend to be shed downstream, with new vortices forming in their stead. These issues result in an increased drag, unsteady loads on the body, and produce an unsteady

wake. Reference [25] presents a trapped vortex cell solution that keeps the vortex near the body at all times, reducing those effects.

3. Solutions to Overcome the Natural Self-Start Inability of Darrieus VAWT

The Darrieus VAWT has a natural inability to self-start, since the blades suffer at the same time with the drag forces and the lift forces. These forces usually balance each other leading to a lack of starting torque. Nevertheless, there are few works that study the starting performance of Darrieus VAWT through the development and validation of computational simulation, as occurs in [26].

Several solutions have been presented to overcome the self-start inability of Darrieus wind turbines, such as external electricity feed-in, guide-vanes, hybrid configuration, blade pitch optimization, blade form optimization, and blade profile design.

3.1. External Electricity Feed-In

The use of a generator with external electricity feed-in helps the rotor to start rotating. This is commonly used in the egg shaped Darrieus VAWT. A problem arises here when the wind turbines are disconnected from the grid and do not have an external electricity source.

3.2. Guide-Vanes

The use of a guide-vane [27] may prevent the drag effect on the blades moving in the upwind zone of the wind turbine, optimizing the wind flow in the downwind zone to maximize the lift forces on the blades. The guide-vanes increase the turbine solidity, leading to higher forces to be exerted in the pole. However, the use of guide-vanes implies that more material and components are required, increasing the VAWT price and reducing its sustainability.

3.3. Hybrid Configuration

A Savonius VAWT has been used in a hybrid configuration with a Darrieus VAWT [28-29]. This hybrid configuration gives the wind turbine the self-start capabilities (offered by the Savonius VAWT) and the ability to operate at TSR higher than one (offered by the Darrieus VAWT). However, at high TSR the Savonius VAWT increases the drag leading to a lower performance, which would not occur if only a Darrieus VAWT was used.

3.4. Blade Pitch Optimization

Reference [30] addresses the VAWT blade pitch optimization. The mechanical systems used to optimize the blade pitch angle are usually complex and, since they need to operate at high speeds when the turbine reaches high TSR, the components experience fatigue. The increase of turbine complexity and components number leads to higher production and maintenance costs. Also, the components fatigue reduces the lifetime of the turbine. Some tools are presented in [15] to define the optimal variation of the blade pitch angle in straight bladed Darrieus VAWT.

3.5. Blade Form Optimization

The optimization of the blade form may increase the drag properties at low TSR and increase the lift properties at high TSR [31]. These systems have similar problems to the blade pitch systems presented earlier, leading to a complexity increase and higher production and maintenance costs.

3.6. Blade Profile Design

A blade profile capable of offering self-start capabilities to the wind turbine is desirable [26]. By studying and developing new profiles for the VAWT blades, a self-start improvement of the wind turbine may be achieved. However, this is a very time consuming task that usually requires a significant computation time to study profile variations. Some of the modifications that can be made to the blade profile to enhance the self-starting behavior of VAWT are: high turbine solidity; blades with inclined leading edge; cambered blades [32-33]; thick blades [34]. However, as the VAWT self-starting behavior is enhanced, a compromise to the wind turbine performance at high TSR should be made.

3.7. Motivation for a New Methodology

This paper envisages the development of new blade profiles to overcome the natural inability of the VAWT to self-start, without compromising much of the performance at high TSR. Several models have been developed to predict the Darrieus VAWT performance when its blades are moving, but no model addresses the study of the turbine ability to self-start relying only on the blades form. Hence, the new methodology presented in this paper offers a fast-computational tool for the development of new blade profiles for Darrieus VAWT, capable of being integrated with existing tools or capable of being used as a standalone tool. The new methodology is presented hereafter.

4. New Methodology to Study Self-Start Capabilities

4.1. The Problem to Solve

To study the self-start capabilities of a VAWT blade profile, there is the need to create a methodology that would give a closer relation between the wind forces acting on the blade, and the blade profile itself. Also, the methodology should be fast in computation time, useful in the first steps of the studies when developing different profile designs.

A wind turbine is able to self-start when without external help (extra components or external energy) it accelerates from a stopped position to a certain rotation movement able to produce energy. The new methodology presented studies the exact moment when the wind turbine starts to move by itself.

The VAWT must take advantage of the drag forces caused by the wind on the blades when the turbine is in a stopped position in order to self-start relying only on the blades profile, without compromising the wind turbine performance at high TSR. If possible, the lift forces should be used in cooperation with the drag forces to induce the self-start capability of the wind turbine, especially when the turbine is stopped and the wind flow starts to achieve higher velocities.

Since the blade may be at any given position around the rotor, there is the need to study the blade profile at any angular position from 0º to 360º. Accordingly, the dynamic stall behavior, air flow separation and any other aerodynamic disturbances must be taken in account [20-22]. To study these aerodynamic disturbances requires a significant computation time, which leads to considerable time consumption not advisable in the first steps of development studies. So, the new methodology that is present here is mainly suitable for a fast analysis, when there is the need to compare several blade profile solutions to start restricting and eliminating different designs. It is also important not to forget the analysis of different aspects of the wind flow disturbances acting on the wind turbine.

4.2. Description of the Methodology

To study the blade profile modifications and the implications that those modifications bring to the wind turbine performance, a close relation between the surface of the blade and the wind flow must be created. In this methodology the pressure coefficient C_{pr} is used, which is a dimensionless number that describes the relative pressure throughout a flow field. It is intimately correlated to the flow velocity, and can be calculated at any point of the flow field.

The C_{pr} is useful to study the forces acting on any given point on the blade profile surface and its relation with dimensional numbers [35] is given by:

$$C_{pr} = \frac{p - p_{\infty}}{1/2\,\rho V_{\infty}^{2}} \tag{24}$$

In a normal operation of a VAWT, the variations of pressure and wind speed have little influence in the wind density, so the wind flow can be treated as being incompressible. Hence, it is assumed that: when C_{pr} is equal to one, that point is a stagnation point, meaning that the flow velocity at that point is null (relevant when optimizing the drag forces); when C_{pr} is negative in the point of study, the wind is moving at a higher speed than in the undisturbed wind flow (relevant when optimizing the lift forces).

To study the C_{pr} around the blade profile surface, firstly there is the need to divide it into segments. The blade profile NACA0020 with surface divisions is shown in Fig. 6. Smaller segments can provide a more accurate analysis.

The pressure coefficient acting on the blade profile divided surface is shown in Fig. 7. This figure illustrates the points i and $i+1$ of the segment of length s in the blade profile surface, their corresponding Cartesian coordinates and the C_{pr} acting on the blade profile surface.

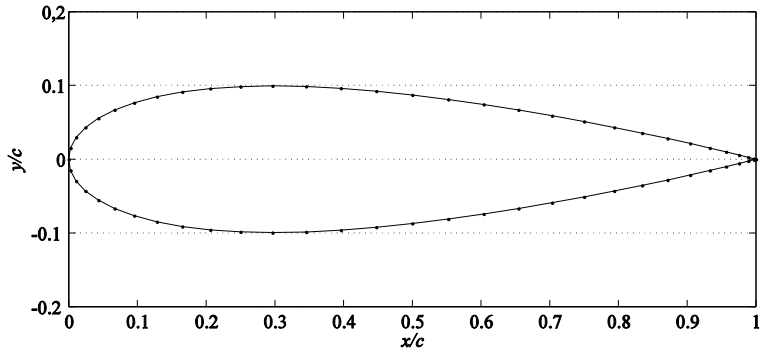

Fig. 6 Blade profile NACA0020 with surface divisions

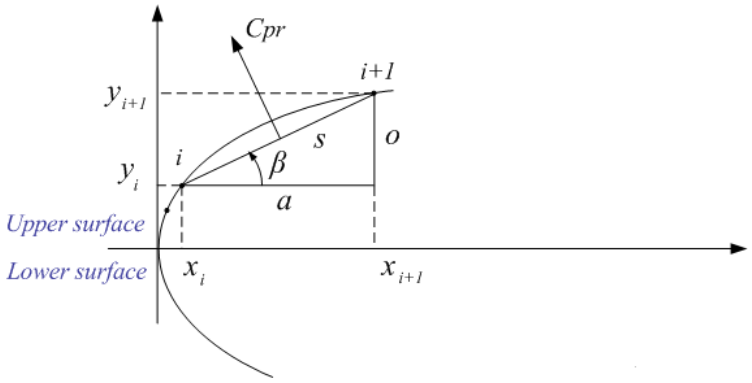

Fig. 7 Pressure coefficient acting on the blade profile divided surface

In order to calculate the length of each segment s there is the need to calculate the length o of the triangles opposite side and the length a of the triangle's adjacent side, which are respectively given by:

$$a = x_{i+1} - x_i \tag{25}$$

$$\begin{cases} o = y_{i+1} - y_i & \text{upper surface} \\ o = y_i - y_{i+1} & \text{lower surface} \end{cases} \tag{26}$$

When $o > 0$ it means that the surface segment is oriented in the direction to the wind turbine rotation. When $o < 0$ the segment is oriented in the opposite direction. The segment length s, and the segment angle β, in relation to the chord axis, are given by:

$$s = \sqrt{a^2 + |o|^2} \tag{27}$$

$$\beta = \arctan\left(\frac{o}{a}\right) \tag{28}$$

The C_{pr} contribution to the forward movement of the wind turbine (the contribution to the tangential force T_{pr}), the C_{pr} contribution to the forces exerted in a radial axis (the contribution to the normal force N_{pr}) and the angle φ of the C_{pr} exerted on the blade surface in relation to the chord line are shown in Fig. 8.

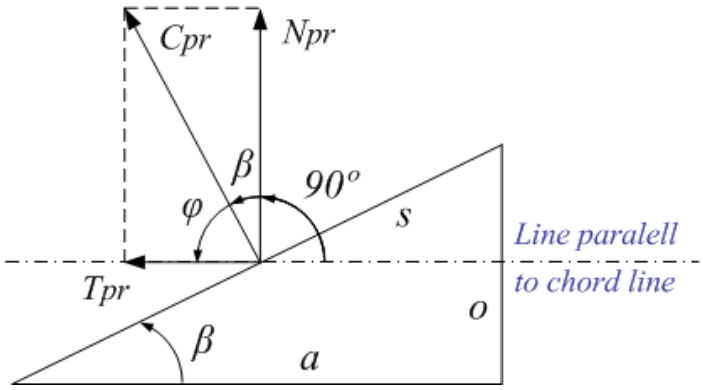

Fig. 8 Pressure coefficient, chordal and normal forces acting on the blade profile surface.

The angle φ of the C_{pr} exerted on the blade surface in relation to the chord line is given by:

$$\varphi = 180^{\circ} - 90^{\circ} - \beta \tag{29}$$

The relationships between C_{pr}, T_{pr}, N_{pr} and φ are given by:

$$\begin{cases} T_{pr} = C_{pr} \cos(\varphi)\, s & \text{when o} \geq 0 \\ T_{pr} = -C_{pr} \cos(\varphi)\, s & \text{when o} < 0 \end{cases} \tag{30}$$

$$\begin{cases} N_{pr} = C_{pr} \sin(\varphi)\, s & \text{upper surface} \\ N_{pr} = -C_{pr} \sin(\varphi)\, s & \text{lower surface} \end{cases} \tag{31}$$

The analysis of the relation between the blade profile design changes and the wind turbine behavior when it's in a stopped position (at any given axial position) is now possible.

5. Case Studies

The new methodology to study the self-start capabilities of the blade profiles for Darrieus type VAWT has been applied on two case studies: one with several symmetrical NACA airfoils, and a second one with asymmetrical airfoils. But, before the analyses are presented, the computational tool used for the C_{pr} calculation will be presented in the next subsection.

5.1. Pressure Coefficient Analyses in Each Blade Airfoil Segment

The aerodynamic behavior and performance data for different blade profiles is not always available, and in the majority of the cases is incomplete. This data is very hard to obtain and it is a very time-consuming task. Several computational fluid dynamics tools are commonly used to generate the aerodynamic performance data needed. The JavaFoil [36] is a fast processing computational tool. The JavaFoil presents several problems at high

angles of attack, but is used in this paper for simplification of presentation and to facilitate the reader data reproducibility.

This computational tool is able to analyze different blade profiles of any configuration, offering all kind of different output data, for instance: velocity and pressure coefficient distribution along the blade chord; lift, drag and momentum coefficient; flow field with pressure vectors; flow stream lines and pressure distribution along the fluid flow; boundary layer evaluation cards; polar card evaluation with the relations between lift and drag coefficients and with the angle of attack variation; and other information. It is also able to evaluate multi-foil and ground effect configurations. One important feature of the JavaFoil is the ability to save all the analysis and output data to a file. Adding the last feature to its integrated scripting module, it is possible to automate the computational processes and to complement the information needs with other tools.

In the theoretical background of the tool, it uses several methods for airfoil analysis, mainly divided in two main areas:

- Potential Flow Analysis. This analysis is done by a panel method with a linear varying vorticity distribution based on XFOIL code. This method is used to calculate the velocity distribution along the surface of the airfoil;
- Boundary Flow Analysis. This analysis is done on the upper and lower surfaces of the airfoil with different equations, starting with the panel method and performing several calculations in a called integral boundary layer method.

Depending on the Reynolds number and other parameters, the tool gives us the ability to choose different analysis methods and configurations, offering more flexibility to the computational processing.

To apply the JavaFoil computational tool for the C_{pr} calculation, a division of the blade path around the rotor and the axial angles in relation to the flow movement is needed. Hence, the rotor division to study the self-start behavior of the VAWT is shown in Fig. 9.

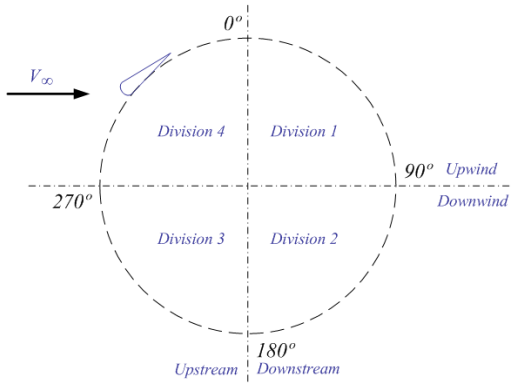

Fig. 9 Rotor division to study the self-start behavior

5.2. Symmetrical Airfoils Analysis

For the symmetrical airfoils data evaluation, the following NACA profiles were selected: NACA0012, NACA0018, NACA0020, NACA0025, and NACA0030.

The NACA0012 and NACA0018 are classical blade profiles used in the VAWT. These profiles are considered to have low self-start capabilities. The thicker NACA0020 blade

profile can be commonly found in the straight-bladed Darrieus wind turbine. The thicker blades show a better self-start performance. The NACA0030 is closer of having self-start capacity nature due to a thicker blade profile. However, a thicker blade leads to an increased drag at high TSR, leading to a performance decrease. The five blade profiles are shown in Fig. 10.

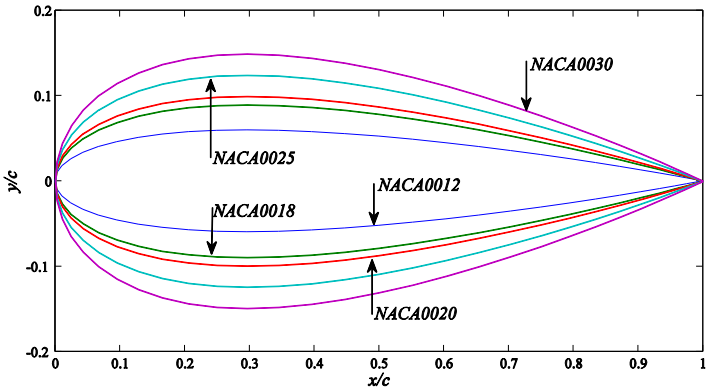

Fig. 10 NACA0012, NACA0018, NACA0020, NACA0025 and NACA0030 blade profiles

In order to apply the proposed methodology, the pressure coefficient needs to be calculated around the blade profile. For the data evaluation presented here, the C_{pr} is calculated for all segments around the blade profile for any given angle between 0º and 360º. The JavaFoil tool offers the pressure coefficient evaluation associated with the x and y coordinates. This evaluation can be automatically performed to the entire 360º at the same time in the velocity area.

By applying (25) and (26) to the given x and y coordinates, the opposite side and the adjacent side are obtained. By applying (27), the length of the airfoil surface exposed to the wind forces can be obtained. Also, using (28) and (29), the C_{pr} angle in relation to the blade chord line φ is determined.

Taking into account all the data previously calculated, it is now possible to determine the C_{pr} contribution to the tangential force T_{pr} and the C_{pr} contribution to the normal force N_{pr}. These forces are related to the actual tangential and normal forces responsible for the blades movement, by the pressure coefficient.

The C_{pr} contribution to the tangential force T_{pr} and the C_{pr} contribution to the normal force N_{pr}, for the chosen NACA airfoils, are shown in Fig. 11 and Fig. 12 respectively.

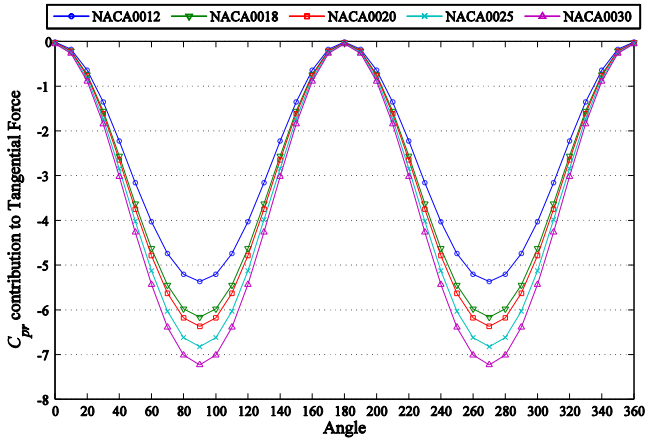

Fig. 11 C_{pr} contribution to the tangential force T_{pr}

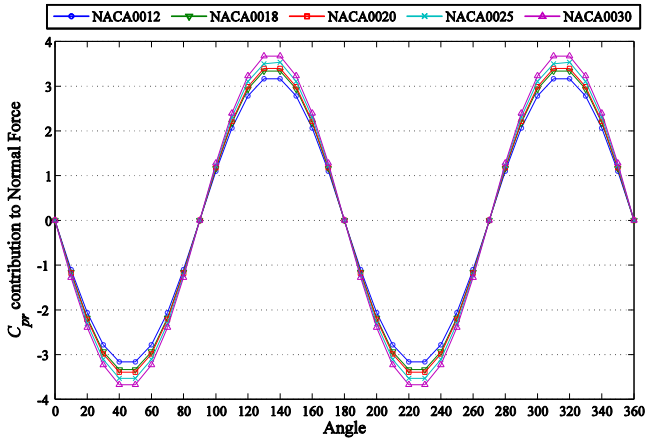

Fig. 12 C_{pr} contribution to the normal force N_{pr}

On one hand, it can be seen in Fig. 11 that a thicker blade implies a higher-pressure coefficient contribution to the forward movement of the wind turbine blades (contribution to the tangential force). Indeed, the NACA0030 presents 26% better performance than the NACA0012. On the other hand, it can be seen in Fig. 12 that the airfoil NACA0012 presents the most desirable behavior. Smaller axial forces imply lesser need of blade/arms connection reinforcements.

When the wind turbine is in a stopped position the drag forces have a considerable contribution to the self-start of the wind turbine. Taking in consideration the divisions shown in Fig. 9, there is the need to increase the drag exerted on the blades when they are positioned in divisions 2 and 3. The pressure coefficient is also used to study the drag contribution to the forward movement of the wind turbines blades. In an incompressible flow, when the pressure coefficient reaches values between one and null, that is a stagnation point. The study of the values that contribute to the forward movement of the wind turbine blades are shown in Fig. 13.

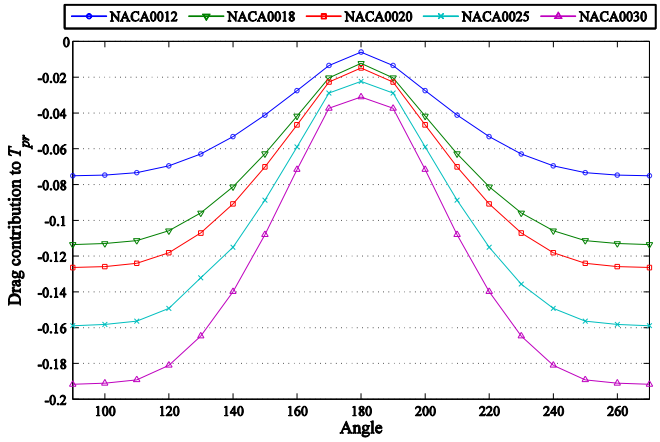

Fig. 13 Drag contribution to the forward movement of the wind turbine blades T_{pr}

In Fig. 13 it can be seen that thicker blades imply higher drag contribution to the forward movement of the wind turbine blades. The drag forces contributing to the tangential force are 150% higher in the NACA0030 than in the NACA0012.

Hence, it was clearly shown that thicker blades are able to provide the wind turbine with self-start capabilities, while the thinner blade wind turbines are most likely unable to self-start.

5.3. Asymmetrical Airfoils Analysis

In asymmetrical airfoils the profile curvature and form may have a direct influence in the wind turbine self-start performance.

To study the influence of the camber size, the NACA0012, NACA2412, NACA4412, NACA6412, NACA8412 and NACA10412 blade profiles were selected, are shown in Fig. 14.

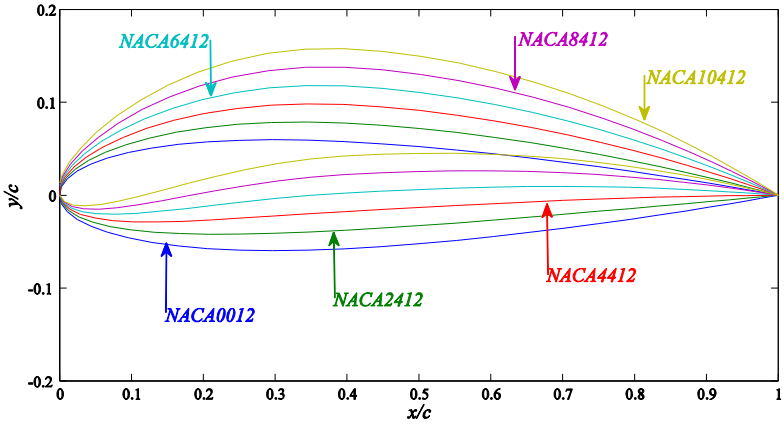

Fig. 14 NACA0012, NACA2412, NACA4412, NACA6412, NACA8412 and NACA10412 blade profiles

All these profiles have 12% of thickness in relation to the chord line size and a camber positioned at 40% of the chord line. The camber sizes in all profiles vary in 2% of the chord line size.

To study the influence of the camber position, the NACA4112, NACA4212, NACA4412, NACA4612, NACA4812 and NACA4912 blade profiles were selected, as shown in Fig. 15.

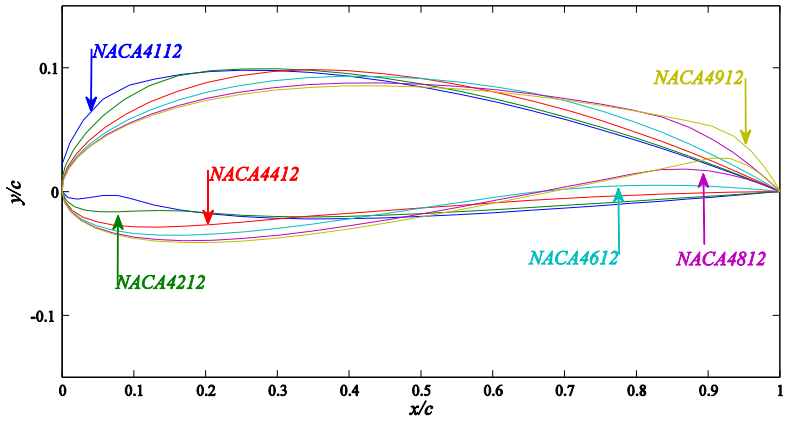

Fig. 15 NACA4112, NACA4212, NACA4412, NACA4612, NACA4812 and NACA4912 blade profiles

All these profiles have 12% of thickness in relation to the chord line size and a camber size of 4% of the chord line size. The profiles vary in the camber position in relation to the chord line at 10%, 20%, 40%, 60%, 80% and 90%, respectively.

The NACA0012 with 12% of thickness, in relation to the blade chord size, and the NACA0018 with 18% of thickness are the classical blade profiles used in the VAWT. These profiles have been studied several times and have a large amount of real measurement data available in the scientific community. These data availability simplifies the prediction simulation, leading to an increased acceptance of these airfoils in the VAWT developments, influencing the acceptance of these profiles in the final turbines. However, these profiles are considered to have low self-start capabilities, for which thicker blades show better performance.

The influence of the camber curvature size and the influence of the camber position are evaluated. The C_{pr} contribution to the tangential force T_{pr} and the C_{pr} contribution to the normal force N_{pr} were calculated, as occurred with the symmetrical airfoils.

The pressure coefficient C_{pr} contribution to the tangential force T_{pr} by varying the blade profile camber curvature size is shown in Fig. 16.

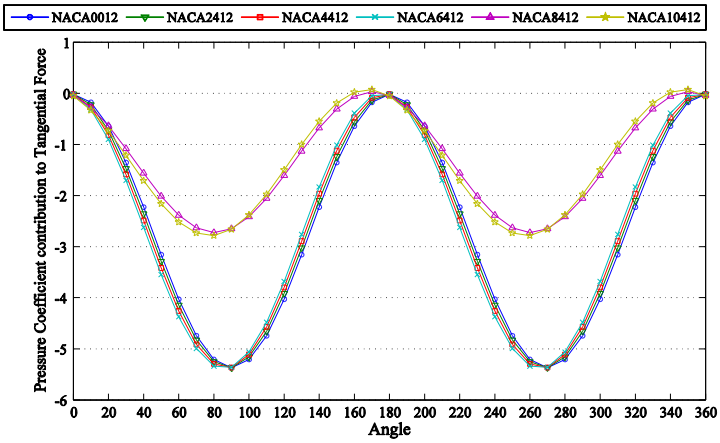

Fig. 16 Pressure coeficiente C_{pr} contribution to the tangential force T_{pr} by varying the blade profile camber curvature size

The pressure coefficient C_{pr} contribution to the tangential force N_{pr} by varying the blade profile camber curvature size is shown in Fig. 17.

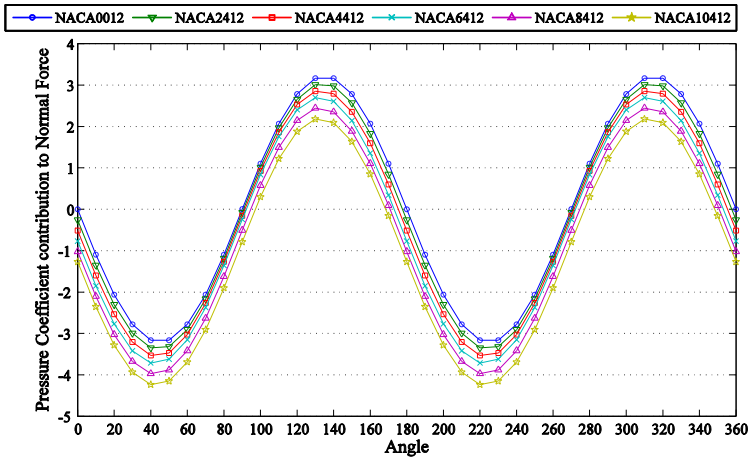

Fig. 17 Pressure coeficiente C_{pr} contribution to the normal force N_{pr} by varying the blade profile camber curvature size

The drag contribution to the forward movement of the wind turbine blades by varying the blade profile camber curvature size is shown in Fig. 18.

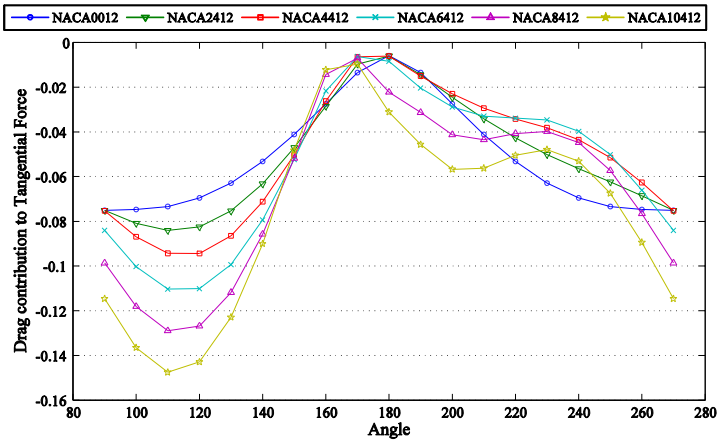

Fig. 18 Drag contribution to the forward movement of the wind turbine blades by varying the blade profile camber curvature size

Fig. 16, Fig. 17 and Fig. 18 presented the airfoil performance evaluation data by applying the new methodology to the variation of the camber curvature size.

The pressure coefficient C_{pr} contribution to the tangential force T_{pr} by varying the blade profile camber position is shown in Fig. 19.

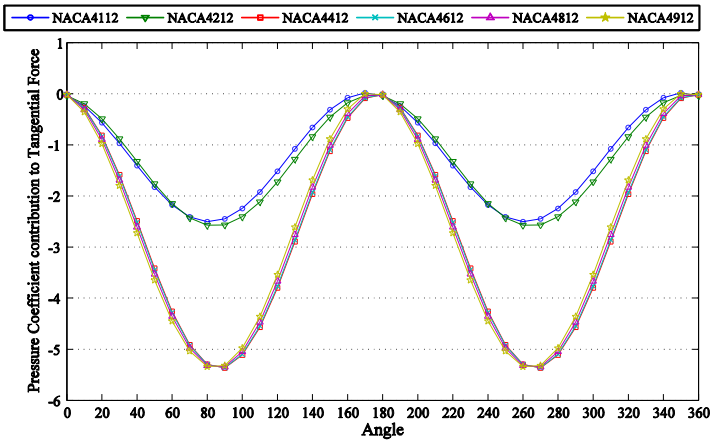

Fig. 19 Pressure coefficient C_{pr} contribution to the tangential force T_{pr} by varying the blade profile camber position

The pressure coefficient C_{pr} contribution to the normal force N_{pr} by varying the blade profile camber curvature size is shown in Fig. 20.

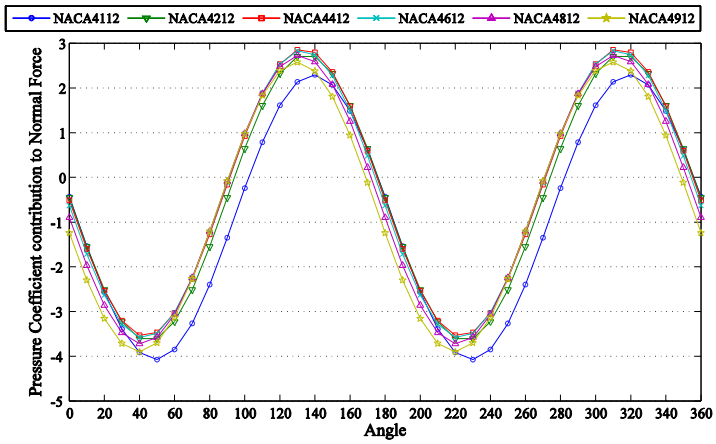

Fig. 20 Pressure coefficient C_{pr} contribution to the normal force N_{pr} by varying the blade profile camber position

The drag contribution to the forward movement of the wind turbine blades by varying the blade profile camber curvature size is shown in Fig. 21.

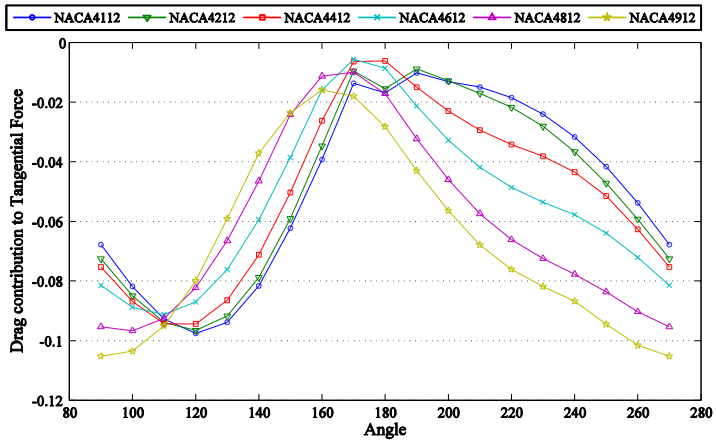

Fig. 21 Drag contribution to the forward movement of the wind turbine blades by varying the blade profile camber position

Fig. 19, Fig. 20 and Fig. 21 presented the airfoil performance evaluation data by applying the new methodology to the variation of the camber position in relation to the airfoil chord.

5.3.1 Camber Curvature Size Variation

In Fig. 16 it can be seen that curvature size doesn't influence the pressure coefficient contribution to the forward movement of the wind turbine blades until it reaches values higher than 6% of the blade chord size. The blade profiles with 8% and 10% sized cambers suffer a performance decrease of 40%.

In Fig. 17 it can be seen that the airfoil NACA0012 presents the most desirable behavior. Smaller axial forces imply lesser need of blade/arms connection reinforcements. Also,

higher camber curvature sizes imply higher displacement of the exerted forces to the outside of the wind turbine and lower to the inside of the rotor.

When the wind turbine is in a stopped position the drag forces have a considerable contribution to the self-start of the wind turbine, especially when the blades are positioned in the downwind side of the rotor.

The pressure coefficient is also used to study the drag contribution to the forward movement of the wind turbine blades. In an incompressible flow, when the pressure coefficient reaches values between one and null, that is a stagnation point. The study of the values that contribute to the forward movement of the wind turbine blades are shown in Fig. 18. It can be seen that higher blade profile camber curvature sizes imply higher drag forces contributing to the forward movement of the wind turbine blades. The airfoil NACA0012 has a symmetrical behavior between the 90º to 180º and 180º to 270º due to its symmetrical shape in the upper and lower airfoil surfaces.

5.3.2 Camber Position Variation

In Fig. 19 it can be seen that when the camber curve is positioned in the first 40% of the blade chord line, a 50% performance decrease occurs compared with the cambers positioned in the last 60% of the blade chord line.

It can be seen in Fig. 20 that the blade chord position does not have a significant influence to the axial exerted forces, except when it is positioned at 10% of the airfoil chord line.

It can be seen in Fig. 21 that the better behaviors are presented by the airfoils that have the cambers positioned in the middle of the chord line.

5.4. Self-start Simulation

In Fig. 22 it can be seen a simulation of a straight blade Darrieus VAWT with 1 m blade and 0.5 m radius. Two wind turbines are compared, one with the symmetrical blade profile NACA0012 and other with the asymmetrical blade profile NACA4412. The simulation is done by the qBlade software [37]. For the of the VAWT start simulation the wind velocity was set to 3 m/s and the wind turbines TSR set to 1.

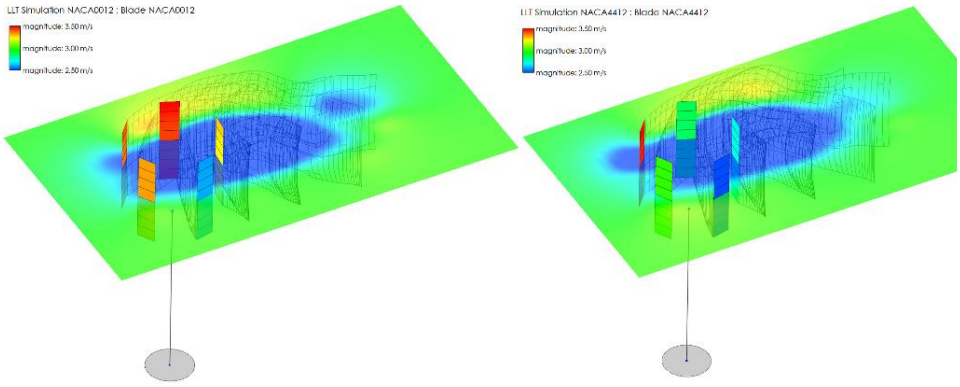

Fig. 22 Symmetrical blade profile NACA0012 and asymmetrical blade profile NACA4412 Darrieus VAWT start simulation

5.5. Blade Development by Applying the New Methodology

A new blade profile for Darrieus VAWT named EN0005 was created by applying the new methodology presented in this paper. The new profile offers self-start to a Darrieus VAWT and good performance at high TSR [32,38-40]. The blade profile EN0005 is presented in Fig. 23.

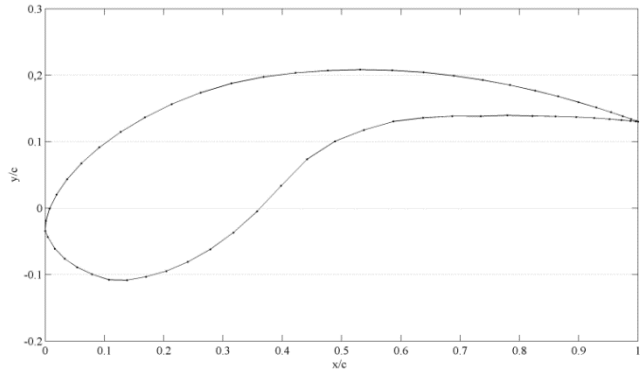

Fig. 23 Blade profile EN0005

The ANSYS FLUENT computational tool is used to generate the aerodynamic performance data presented in the following analysis and comparison instead of the JavaFoil, since it presents a more accurate and validated good accuracy although more difficult to use.

In Fig. 24 and Fig. 25 the blade profile EN0005 C_{pr} contribution to the T_{pr} and N_{pr} respectively is compared with the symmetrical profiles NACA0018 and NACA0020 and asymmetrical profiles NACA4418 and NACA4420 same data.

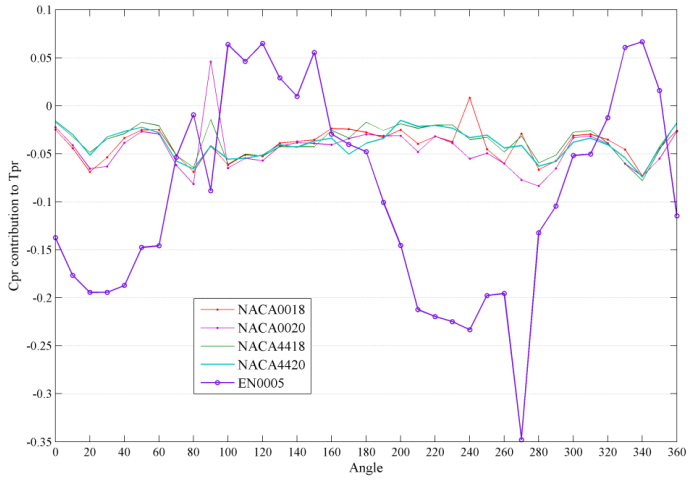

Fig. 24 C_{pr} contribution to the tangential force T_{pr}

Fig. 24 shows a better capability for the blade profile EN0005 to offer self-start capability to the Darrieus VAWT. From angle 0º to 80º and 180º to 310º The EN0005 blade profile

presents a better contribution to the lift force. Also, the EN0005 presents a drag force contributing for the forward movement of the Darrieus VAWT between the angles 100º and 150º and presents a lower variation in the normal force between the 70º and 180º. Although with inversed orientation for the remaining angles, the normal force is very similar to the other blade profiles. The self-start ability that blade profile EN0005 offers is validated in the independent work [32].

Fig. 25 C_{pr} contribution to the normal force N_{pr}

6. Conclusion

- This paper focused on the study and development of new blade profiles for Darrieus type VAWT capable to self-start without the use of extra components or external energy input. A new methodology for fast development and its associated equations have been presented, in order to study the influences of the wind on the turbine in its stopped position. This new methodology gives a close relation between the blade profile design and the wind forces acting on the blades.
- Two caste studies were provided: one with symmetrical NACA airfoils and other with asymmetrical airfoils. In the asymmetrical airfoils, a closer study to the camber curvature size and position has also been presented. The comprehensive results obtained from the two case studies are in very good agreement with other works in the scientific community, validating the proficiency and usefulness of the proposed methodology.
- A real case of a new blade profile developed with the methodology presented in this paper is shown. The new blade profile called EN0005 presents the ability to offers self-start capabilities to a Darrieus VAWT.

Acknowledgment

This work is funded by: European Union through the European Regional Development Fund, included in the COMPETE 2020 (Operational Program Competitiveness and

Internationalization) through the ICT project (UID/GEO/04683/2013) with the reference POCI010145FEDER007690; Portuguese Funds through the Foundation for Science and Technology-FCT under the project LAETA 2015-2020, reference UID/EMS/50022/2013; Portuguese Foundation for Science and Technology (FCT) under Project UID/EEA/04131/2013.

Nomenclature

A	Area swept by the wind turbine	Q	Turbine overall torque
a	Blade profile surface segment adjacent	r	Turbine rotor radius
c	Blade profile chord	R_e	Reynolds number
C_d	Blade drag coefficient	s	Blade profile surface segment
C_D	Turbine drag coefficient	T_{pr}	Pressure coefficient contribution to the tangential force
C_l	Blade lift coefficient	V_∞	Undisturbed wind velocity
C_m	Blade momentum coefficient	V_a	Induced velocity
C_P	Power coefficient	V_r	Induced velocity due to the rotor angular speed at the wind turbine
C_{pr}	Pressure coefficient	V_c	Chordal velocity component
C_{prl}	Pressure coefficient in the lower surface	V_n	Normal velocity component
C_{pru}	Pressure coefficient in the upper surface	V_{au}	Induced velocity in the upstream
C_Q	Turbine overall torque coefficient	V_{ad}	Induced velocity in the downstream
C_t	Tangential force coefficient	V_e	Wake velocity in the upstream
C_n	Normal force coefficient	V_w	Wake velocity in the downstream
D	Blade drag force	u_d	Interference factor for the downstream
F_D	Turbine drag force	u_u	Interference factor for the upstream
F_t	Tangential force	W	Relative flow velocity
F_n	Normal force	α	Blade angle of attack
F_{ta}	Average tangential force	β	Blade profile surface segment angle in relation to the chord line
h	Turbine height	γ	Blade pitch angle
k	Factor found by iteration	θ	Blade azimuth angle around the rotor
L	Blade lift force	ρ	Fluid density
n	Number of blades	λ	Tip speed ratio
N_{pr}	Pressure coefficient contribution to the normal force	μ	Dynamic viscosity of the fluid
o	Blade profile surface segment opposite	σ	Turbine solidity
P	Turbine overall power	ν	Kinematic viscosity of the fluid
p	Pressure of the point where the evaluation of the pressure coefficient is made	φ	Pressure coefficient angle in relation to the chord line
p_∞	Pressure of the undisturbed wind	ω	Rotor angular speed at the wind turbine

References

[1] Francese D., Adamo E., Khanmohammadi S. Micro-aeolic in residential districts: a Case study in Sant'Arsenio (south-western Italy). Mediterranean Green Buildings and Renewable Energy 2017; 369-377.

[2] Jäger-Waldau A. PV Status Report 2017. Publications Office of the European Union 2017.

[3] Melicio R., Mendes V.M.F., Catalão J.P.S. Computer simulation of wind power systems: power electronics and transient stability analysis. Proceedings of the Int. Conference on Power Systems Transients (IPST 2009), 1–7, Kyoto, Japan, June 2009.

[4] Batista N.C., Melicio R., Matias J.C.O, Catalão J.P.S. ZigBee standard in the creation of wireless networks for advanced metering infrastructures. Proceedings of the 16th IEEE Mediterranean Electrotechnical Conference, 220–223, Medina Yasmine Hammamet, Tunisia, March 2012. https://doi.org/10.1109/MELCON.2012.6196418

[5] Melicio R., Mendes V.M.F., Catalão J.P.S. Modeling, control and simulation of full-power converter wind turbines equipped with permanent magnet synchronous generator. International Review of Electrical Engineering 2010; 5(2): 397-408.

[6] Melicio R., Mendes V.M.F., Catalão J.P.S. Modeling and simulation of wind energy systems with matrix and multilevel power converters. IEEE Latin America Transactions 2009; 7(1): 78-84. https://doi.org/10.1109/TLA.2009.5173468

[7] Arab A., Javadi M., Anbarsooz M., Moghiman M. A numerical study on the aerodynamic performance and the self-starting characteristics of a Darrieus wind turbine considering its moment of inertia. Renewable Energy 2017; 107: 298-311. https://doi.org/10.1016/j.renene.2017.02.013

[8] D'Alessandro V., Montelpare S., Ricci R., Secchiaroli A. Unsteady aerodynamics of a Savonius wind rotor: a new computational approach for the simulation of energy performance. Energy, 2010; 35: 3349-3363. https://doi.org/10.1016/j.energy.2010.04.021

[9] Shigetomi A., Murai Y., Tasaka Y., Takeda Y.. Interactive flow field around two Savonius turbines. Renewable and Sustainable Energy Reviews, 2011; 36: 536-545. https://doi.org/10.1016/j.renene.2010.06.036

[10] Hill N., Dominy R., Ingram G., Dominy J. Darrieus turbines: the physics of self-starting. Proceedings of the Institution of Mechanical Engineers, Part A: Journal of Power and Energy, 2009; 223: 21 – 29. https://doi.org/10.1243/09576509JPE615

[11] Castelli M.R., Englaro A., Benini E. The Darrieus wind turbine: proposal for a new performance prediction model based on CFD. Energy, 2011; 36: 4919 – 4934. https://doi.org/10.1016/j.energy.2011.05.036

[12] Kjellin J., Bulow F., Eriksson S., Deglaire P., Leijon M., Bernhoff H. Power coefficient measurement on a 12 kW straight bladed vertical axis wind turbine. Renewable Energy, 2011; 36: 3050 – 3053. https://doi.org/10.1016/j.renene.2011.03.031

[13] Islam M., Ting D.S.K., Fartaj A. Aerodynamic models for Darrieus-type straight-bladed vertical axis wind turbines. Renewable and Sustainable Energy Reviews, 2008; 12: 1087 – 1109. https://doi.org/10.1016/j.rser.2006.10.023

[14] Ponta F.L., Seminara J.J., Otero A.D. On the aerodynamics of variable-geometry oval-trajectory Darrieus wind turbines. Renewable Energy, 2007; 32: 35 – 56. https://doi.org/10.1016/j.renene.2005.12.007

[15] Paraschivoiu I., Trifu O., Saeed F. H-Darrieus wind turbine with blade pitch control. Int J Rotating Machinery, 2009; 2009: 1 – 7. https://doi.org/10.1155/2009/505343

[16] Batista N.C., Melicio R., Mendes V.M.F., Figueiredo J., Reis A.H. Darrieus wind turbine performance prediction: computational modeling. Technological Innovation for the Internet of Things, SPRINGER, Heidelberg, Germany, April 2013; 382-391.

[17] Gazzano R., Marini M., Satta A. Performance calculation for a vertical axis wind turbine with variable blade pitch. Int J Heat and Technology, 2010; 28: 147 – 153.

[18] Anderson F., Fletcher T.M., Brown R.E. Simulating the aerodynamic performance and wake dynamics of a vertical-axis wind turbine. Wind Energy, 2011; 14: 159 – 177. https://doi.org/10.1002/we.409

[19] Islam M., Amin M.R., Ting D.S.K., Fartaj A. Aerodynamic factors affecting performance of straight-bladed vertical axis wind turbines. Proceedings of the ASME Int Mechanical Engineering Congress and Exposition, Washington, USA, November, 2007. https://doi.org/10.1115/IMECE2007-41346
[20] Ferreira C.S., van Kuik G., van Bussel G., Scarano F. Visualization by PIV of dynamic stall on a vertical axis wind turbine. Experiments in Fluids, 2009; 46: 97 – 108. https://doi.org/10.1007/s00348-008-0543-z
[21] Ferreira C.J.S., van Zuijlen A., Biji H., van Bussel G., van Kuik G. Simulating dynamic stall in a two-dimensional vertical-axis wind turbine: verification and validation with particle image velocimetry data. Wind Energy, 2010; 13: 1 – 17. https://doi.org/10.1002/we.330
[22] Greenblatt D., Schulman M., Ben-Harav A. Vertical axis wind turbine performance enhancement using plasma actuators. Renewable Energy, 2012; 37: 345 – 354. https://doi.org/10.1016/j.renene.2011.06.040

[23] Balduzzi F., Bianchini A., Carnevale E.A., Ferrari L., Magnani S. Feasibility analysis of a Darrieus vertical-axis wind turbine installation in the rooftop of a building. Applied Energy, 2012; 97: 921 – 929. https://doi.org/10.1016/j.apenergy.2011.12.008
[24] Qin N., Howell R., Durrani N., Hamada K., Smith T. Unsteady flow simulation and dynamic stall behaviour of vertical axis wind turbine blades. Wind Engineering, 2011; 35: 511-527. https://doi.org/10.1260/0309-524X.35.4.511
[25] Zannetti L., Gallizio F., Ottino G. Vortex capturing vertical axis wind turbine. J of Physics Conf Series, 2007; 75: 1-10. https://doi.org/10.1088/1742-6596/75/1/012029
[26] Dominy R., Lunt P., Bickerdyke A., Domniny I. Self-starting capability of a Darrieus turbine. Proc Inst Mech Eng Part A-J Power Energy, 2007; 211: 111-120. https://doi.org/10.1243/09576509JPE340
[27] Shahizare B., Nik-Ghazali N., Chong W.T., Tabatabaeikia S., Nima I., Alireza E. Novel investigation of the different Omni-direction-guide-vane angles effects on the urban vertical axis wind turbine output power via three-dimensional numerical simulation. Energy Conversion and Management, 2016; 117: 206–217. https://doi.org/10.1016/j.enconman.2016.03.034
[28] Xiaoting L., Sauchung F., Baoxing O., Chili W., Christopher C., Kaihong P. A computational study of the effects of the radius ratio and attachment angle on the performance of a Darrieus-Savonius combined wind turbine. Renewable Energy, 2017; 113: 329-334. https://doi.org/10.1016/j.renene.2017.04.071
[29] Bhuyan S., Biswas A. Investigations on self-starting and performance characteristics of simple H and hybrid H-Savonius vertical axis wind rotors. Energy Conversion and Management, 2014; 87: 859-867. https://doi.org/10.1016/j.enconman.2014.07.056
[30] Chen J.S.J., Chen Z., Biswas S., Miau J.J., Hsieh C.H. Torque and power coefficients of a vertical axis wind turbine with optimal pitch control. Proceedings of the ASME 2010 Power Conference, Illinois, USA, July, 2010. https://doi.org/10.1115/POWER2010-27224
[31] Bhatta P., Paluszek M.A., Mueller J.B. Individual blade pitch and camber control for vertical axis wind turbines. Proceedings of the World Wind Energy Conf 2008, Kingston, Canada, June, 2008.
[32] Sengupta A.R., Biswasa A., Guptab R. Studies of some high solidity symmetrical and unsymmetrical blade H-Darrieus rotors with respect to starting characteristics, dynamic performances and flow physics in low wind streams. Renewable Energy 2016; 93: 536-547. https://doi.org/10.1016/j.renene.2016.03.029
[33] Sayyad B.Q., Isam J. Investigation of effect of cambered blades on Darrieus VAWTs. Energy Procedia 2017; 105: 537-543. https://doi.org/10.1016/j.egypro.2017.03.353
[34] Chi-Cong N., Thi-Hong-Hieu L., Phat-Tai T. A numerical study of thickness effect of the symmetric NACA 4-digit airfoils on self starting capability of a 1 kW H-type vertical axis wind turbine. International Journal of Mechanical Engineering and Applications. Special Issue: Transportation Engineering Technology — part II. 2015; 3: 7-16.
[35] Anderson J.D. Fundamentals of aerodynamics, McGraw-Hill Series in Aeronautical and Aerospace Engineering, New York, NY, USA,2010.
[36] Hepperle M. JavaFoil – Analysis of Airfoils. Available: http://www.mh-aerotools.de/.

[37] Marten D., Wendler J., Pechlivanoglou G., Nayeri C.N., Paschereit C.O. Qblade: an open source tool for design and simulation of horizontal and vertical axis wind turbines. Emerging Technology and Advanced Engineering 2013; 3: 264-269.
[38] Batista N.C., Melicio R., Mendes V.M.F., Calderón M., Ramiro A.. On a self-start Darrieus wind turbine: Blade design and field tests. Renewable and Sustainable Energy Reviews 2015; 52: 508-522. https://doi.org/10.1016/j.rser.2015.07.147
[39] Batista N.C., Melicio R., Catalão J.P.S. Vertical axis turbine blades with adjustable form. Patent US 2012/0163976A1; 2012.
[40] Batista N.C., Melicio R., Matias J.C.O, Catalão J.P.S. New blade profile for Darrieus wind turbines capable to self-start. Proceedings of the Renewable Power Generation Conference, 1–5, Edinburgh, UK, September 2011. https://doi.org/10.1049/cp.2011.0219